

3D-OGSE: Online Smooth Trajectory Generation for Quadrotors using Generalized Shape Expansion in Unknown 3D Environments

Vrushabh Zinage¹, Senthil Hariharan Arul² and Dinesh Manocha²

Abstract—In this letter, we present an online motion planning algorithm for generating smooth, collision-free trajectories for quadrotors operating in an unknown, cluttered 3D environment. Our approach constructs a non-convex safe-region termed generalized shape at each timestep, which represents the obstacle-free region in the environment. A collision-free path is computed by sampling points in the generalized shape and is used to generate a smooth, time-parameterized trajectory by minimizing snap. The generated trajectories are constrained to lie within a convex subset of the generalized shape, which ensures the quadrotor maneuvers in the local obstacle-free space. This process is repeated at each timestep to re-plan trajectories until the quadrotor reaches its goal position. We evaluate the proposed method in simulation on complex 3D environments with high obstacle densities. We observe that each re-planning computation takes ~ 1.6 milliseconds on a single thread of an Intel Core i5-8500 3.0 GHz CPU. In addition, our method is 6 – 10x faster than prior online motion planning methods, and we observe less conservative behavior in complex scenarios such as narrow passages.

I. INTRODUCTION

Due to their small size and superior agility, UAVs (unmanned aerial vehicles) are increasingly being used for various applications including search and rescue, surveillance, and exploration. A key problem is generating smooth, feasible trajectories for a UAV agent, especially for dense or cluttered 3D environments. In many scenarios, the operating environment is unknown prior to the flight [1], [2] and therefore it is not possible to pre-compute a collision-free trajectory. As a result, we need efficient online planning algorithms that can rapidly compute a collision-free, dynamically feasible trajectory using only local sensor data.

There has been extensive research over the last decade on trajectory generation for UAVs [3], [4], [5]. At a broad level, prior trajectory generation methods can be grouped into three categories: (1) optimization-based algorithms [5], [6]; (2) search-based/motion primitives [7], [8], [9]; and (3) sampling-based methods [10], [11]. Most of these algorithms do not provide real-time performance in dense, unknown 3D scenarios.

Many techniques [3], [12], [11] have been proposed to pre-compute collision-free paths for a UAV agent in environments with static obstacles. However, these methods may not work well in unmapped environments. Others rely on generating a safe corridor for an agent to compute a collision-free trajectory, but often such methods [13], [14] approximate the free space as a convex shape to reduce the complexity

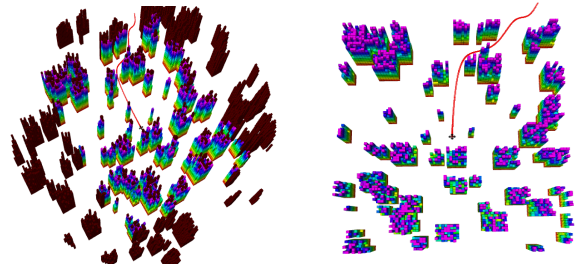


Fig. 1: A quadrotor maneuvering a random forest environment using 3D-OGSE. The quadrotor has a sensing region of 10m x 10m, and the multicolored obstacles represent the obstacles inside the agent's sensing region. The brown obstacles are not visible to the agent at the current instance. The red curve represents the planned trajectory. Our approach can handle dense 3D environments.

and enable fast computation. In practice, these methods can be very conservative, especially in complex scenarios with narrow passages.

Main Contributions: We present 3D-OGSE, an online motion planning algorithm for generating collision-free, smooth trajectories for quadrotors operating in unknown, obstacle cluttered 3D environments (Fig. 1). Our method is based on 3D-GSE [15], an offline algorithm for collision-free planning in known 3D environments. We present a significant extension that computes the 3D-GSE in an online manner using local depth information of complex 3D environments and re-plans trajectories when necessary. Our approach is based on computing planar projections from the 3D obstacles point cloud data, and uses a combination of point samples and conic hulls to compute a good approximation of the obstacle-free space. Our novel components include:

1. Online 3D-GSE Computation and Replanning triggering strategy: We present a fast technique to compute the 3D-GSE in an online manner using the local depth information from a depth sensor. Since, we have knowledge only about the local environment, we treat the unexplored region as a obstacle-free space. In addition, we present an efficient online replanning strategy based on the notion of generalized shape which replans only when necessary and not at regular intervals as new point cloud is received (Section IV-C).

2. Dynamically Feasible Time Parametrized Trajectories: We compute time parameterized smooth trajectories using snap minimization, which guarantees smooth and efficient maneuvering for a quadrotor agent. In order to perform fast computations and avoid local minima issues, we use a convex subset of the 3D-GSE for trajectory computation.

¹Vrushabh Zinage is with Department of Aerospace Engineering, Indian Institute of Technology Madras, Chennai, India ael6b017@smail.iitm.ac.in

²Senthil Hariharan Arul and Dinesh Manocha are at University of Maryland, College Park, USA dm@cs.umd.edu

This enables our method to handle complex and cluttered 3D environments with narrow passages (Section V).

Our approach is fast, and the re-planning algorithm takes less than 1.6ms on a single Intel core i5-8500 3.0 GHz CPU, thereby making it suitable for online trajectory generation in unknown environments. In practice, our approach is 6 – 10x faster than prior methods [13], [14] and can handle complex 3D environments with narrow passages (Section V).

II. RELATED WORK

In this section, we summarize the related work in the areas of path planning and online trajectory generation.

Optimization methods: Mixed-integer optimization methods [5], [6] are commonly used to generate reliable, collision-free, dynamically feasible trajectories for quadrotors, but they have high computational overhead and cannot be used for online scenarios. Chen et al. [4] and Augugliaro et al. [3] rely on Sequential Convex Programming (SCP) to generate smooth trajectories. These methods have been mainly used in known environments; due to high computation cost they are not suitable for fast online trajectory generation. Mellinger et al. [16] propose a minimum snap formulation that uses differential flatness and pose the trajectory generation problems as QP (Quadratic program) problems. Online 3D trajectories can be generated using QP methods [13], [14]. These techniques use convex safe corridors and provide a considerable performance improvement over mixed-integer methods. Zucker et al. [17] formulate the trajectory generation problem as a nonlinear optimization over penalty of smoothness and safety to obtain a locally optimal solution; this method has been successfully tested on quadrotors [18].

Search-based methods: Search-based planning methods [7], [8], [9] are used for the fast generation of trajectories for UAVs. They build a graph by discretizing the state space of the UAVs, where the state forms the node, and the motion primitives form the edges in the graph. These methods rely on searching a large pre-computed lookup table that contains the motion primitive to identify the suitable maneuver. Liu et al. [19] avoid using the large lookup table when they plan in the lower dimensional flat state space by harnessing the differential flatness property of the quadrotor.

Sampling-based methods: Many sampling methods like PRM [20] and RRT [21] have been used for collision-free path computation. Sampling-based methods such as [11], [10], [12] avoid the explicit construction of configuration space and have been successfully used for collision-free path computation in high dimensional configuration spaces. These methods compute sampling points in the free space and tend to grow the graph towards the goal configuration. Karaman and Frazzoli [10] propose RRT* and PRM*, which provide asymptotic optimality. Our method is also based on a sampling-based approach, but we avoid exact 3D collision checking as that is regarded as one of the major bottlenecks in prior sampling-based algorithms. Instead, we approximate the obstacle-free region using 3D-GSE and using sample points in the configuration space to compute collision-free paths in the workspace.

Dynamics Constraints: Smooth trajectories for a quadrotor

Notations	Description
\mathbb{X}, \mathbf{X}	3D workspace and a point in 3D workspace, respectively
\mathbb{V}, \mathbb{E}	Vertex and edge set, respectively
m_{loc}	Number of obstacles after segmentation of local map in \mathbb{X}
\mathbf{p}	Current position of quadrotor
$r_{i,\mathbf{X}}$	Minimum distance of \mathbf{X} from obstacle i
$p_{i,\mathbf{X}}$	Point on obstacle i at a distance of $r_{i,\mathbf{X}}$ from \mathbf{X}
$\mathbf{n}_{i,\mathbf{X}}$	Vector from \mathbf{X} to $p_{i,\mathbf{X}}$
$\mathbb{Q}_{i,\mathbf{X}}$	Set of points of intersection of plane with normal $\mathbf{n}_{i,\mathbf{X}}$ and passing through $p_{i,\mathbf{X}}$ and the lines joining the points on obstacle i and \mathbf{X}
$l_{i,\mathbf{X}}$	Maximum distance of point $p_{i,\mathbf{X}}$ from the points in $\mathbb{Q}_{i,\mathbf{X}}$
$\mathcal{G}_{\mathbf{X}}$	3D generalized shape about \mathbf{X}
$\mathcal{R}_{i,\mathbf{X}}$	Spherical sector with vertex at the sampled point \mathbf{X} radius equal to $r_{i,\mathbf{X}}$, cone angle equal to $\tan^{-1}(l_{i,\mathbf{X}}/r_{i,\mathbf{X}})$ and axis along $\mathbf{n}_{i,\mathbf{X}}$
$\widetilde{\mathcal{R}}_{i,\mathbf{X}}$	Intersection of \mathbb{X} and the spherical sector with vertex at sampled point \mathbf{X} , cone angle $\tan^{-1}(l_{i,\mathbf{X}}/r_{i,\mathbf{X}})$, axis along $\mathbf{n}_{i,\mathbf{X}}$ and radius being infinite
$\widetilde{\mathcal{R}}_{ij,\mathbf{X}}$	$\widetilde{\mathcal{R}}_{i,\mathbf{X}} \cap \widetilde{\mathcal{R}}_{j,\mathbf{X}}$ for $i < j$

TABLE I: Symbols used in the paper.

are generated by minimizing jerk [22] and snap [16] by exploiting the differential flatness property. Many methods, such as [3], [4], [23] use Sequential Convex Programming (SCP) to generate smooth trajectories. SCP based methods are generally computationally expensive and are not preferred for fast online trajectory generation. Zhu et al. [24] and Kamel et al. [25] generate local collision-free trajectories and provide control of quadrotors using a Non-linear Model Predictive Controller. In our method, we choose an approach similar to [16] for generating a snap minimized trajectory from a set of waypoints.

III. PRELIMINARIES

In this section, we define the notation used in the paper, discuss our assumptions, and present our mathematical formulation of the problem. A list of symbols used in our paper and their definitions is given in Table I.

A. Assumptions on the Agent and Environment

We assume that the quadrotor is equipped with a depth camera and can access the point cloud information about the local environment within its sensing region. The 3D point cloud data is gathered in an online manner and is the input to our algorithm. Additionally, we assume that the agent can segment the point cloud into distinct obstacles in the environment. Many computer vision and geometry processing techniques such as [26], [27], [28] perform similar real-time segmentation. Finally, we assume that the agent can localize itself in the environment.

B. Differential flatness

A nonlinear system given by $\dot{\mathbf{x}} = f(\mathbf{x}, \mathbf{u})$ is differentially flat if there exists a set $\boldsymbol{\tau}$ (flat output) whose elements, expressed as $\boldsymbol{\tau} = [\tau_1, \tau_2, \tau_3, \dots, \tau_m]$, are differentially independent and whose derivatives can be used to construct the system state space and control inputs [29], [30]. The quadrotor model we consider is described below; from [16] we know the quadrotor dynamics is differentially flat for the flat output set given by $\boldsymbol{\tau} = [\tau_1, \tau_2, \tau_3, \tau_4] = [x, y, z, \psi]$.

Quadrotor model: The state space and the control input are

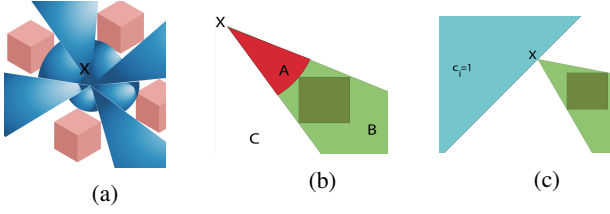


Fig. 2: Fig. (a): A representative 3D generalized shape about point \mathbf{X} . Fig. (b): \mathbf{A} is inside the spherical sector $R_{i,X}$, \mathbf{B} is outside the spherical sector, but inside the conic hull of $R_{i,X}$ and \mathbf{C} is outside the conic hull. $h_i = 2$ if and only if the point belongs to the spherical sector and $f_i = 1$ if and only if the point is outside the conic hull of the spherical sector. Fig. (c): Generating convex subset of g_i . The yellow region shows the conic hull of $\mathcal{R}_{i,X}$ constructed about the point \mathbf{X} .

given by:

$$\mathbf{x} = [x, y, z, \dot{x}, \dot{y}, \dot{z}, \phi, \theta, \psi, p, q, r]$$

$$\mathbf{u} = [T, \dot{\phi}, \dot{\theta}, \dot{\psi}]$$

As in [16], we consider the flat output set given by $\boldsymbol{\tau} = [x, y, z, \phi]$ for our quadrotor system.

C. Generalized Shape: 2D-GSE and 3D-GSE

The basic idea of computing the GSE in 2D and 3D is described by Zinage et al. [12], [15]. They present an offline-method to generate collision-free trajectories for an agent using non-convex safe regions in 2D and 3D environments. These safe regions are labeled as generalized shapes (GSE) and used to compute collision-free paths by sampling points. We use the same notion of GSE, but present techniques to extend the 3D-GSE to perform computations in an online manner for unknown environments. For a detailed handling of the 3D-GSE algorithm, refer to [15]. Consider an agent at a point \mathbf{p} in the 3D environment. Let there be m_{loc} obstacles in the workspace.

For each obstacle $i \in \{1, 2, \dots, m_{\text{loc}}\}$ in the local map, we now have the parameters $r_{i,X}$, $l_{i,X}$, and $\mathbf{n}_{i,X}$ (refer to Table I) computed about \mathbf{X} . Without loss of generality we assume that $r_{1,X} \leq r_{2,X} \dots r_{m_{\text{loc}},X}$.

$$\mathcal{G}_X = \mathcal{R}_{1,X} \cup (\mathcal{R}_{2,X} - \widetilde{\mathcal{R}_{12,X}}) \cup (\mathcal{R}_{3,X} - (\widetilde{\mathcal{R}_{23,X}} + \widetilde{\mathcal{R}_{13,X}}))$$

$$\cup \dots \cup (\mathcal{R}_{m,X} - \cup_{j=1}^{j=i-1} \widetilde{\mathcal{R}_{jm,X}}) \cup \mathcal{I}, \quad (1)$$

where, the set \mathcal{I} is given as, $\mathcal{I} \subset \mathbb{X} | \mathcal{I} \cap \{\cup_{i=1}^{i=m_{\text{loc}}} \widetilde{\mathcal{R}_{i,X}}\} = \emptyset$. Equation 1 provides the geometric representation of the non-convex generalized shape for a general case with m_{loc} obstacles.

D. Problem Formulation

Consider a 3D environment denoted by $\mathbb{X} \subset \mathbb{R}^3$. In the rest of the paper, we assume that a quadrotor is a point object. Our approach can be easily extended to deal with quadrotor geometry by assuming a spherical bounding volume and ensuring a minimum distance (given by radius

of the bounding sphere) between the point robot and the obstacles. Let the obstacle workspace be $\mathbb{X}_{\text{obs}} \subset \mathbb{X}$. Hence, the obstacle-free space for the agent is given by $\mathbb{X}_{\text{free}} = \mathbb{X} \setminus \mathbb{X}_{\text{obs}}$. Given an initial state $\mathbf{X}_{\text{init}} \in \mathbb{X}_{\text{free}}$ and a goal state $\mathbf{X}_{\text{goal}} \in \mathbb{X}_{\text{free}}$, the task is to re-plan a time parameterized trajectory $\sigma(t)$ at each timestep based on the local depth information, until the quadrotor reaches the goal. Furthermore, our formulation ensures that the total snap incurred $c(\sigma(t))$ by the quadrotor is minimized. The dynamical model for the quadrotor is taken from [31]. The corresponding mathematical optimization problem can be expressed as:

$$\begin{aligned} & \underset{\sigma(t)}{\text{minimize}} \quad c(\sigma(t)) \\ & \text{subject to} \quad \sigma(t_0) = \mathbf{X}_{\text{init}}; \quad \sigma(t_h) = \mathbf{X}_{\text{goal}} \\ & \quad \|\dot{\sigma}(t)\| \leq \mathbf{v}_{\text{max}}; \quad \|\ddot{\sigma}(t)\| \leq \mathbf{a}_{\text{max}} \\ & \quad \sigma(t) \in \mathbb{X}_{\text{free}}; \quad \forall t \in [t_0, t_h] \end{aligned} \quad (2)$$

where t_0 is the initial time and t_h is the time at which the agent reaches the goal, where $\sigma(t) : [t_0, t_h] \rightarrow \mathbb{R}^3 \times SO(2)$ and $SO(2)$ is the special orthogonal group of dimension 2. The cost function $c(\sigma(t))$ represents the total snap for the generated trajectory.

IV. 3D-OGSE: ONLINE TRAJECTORY GENERATION

In this section, we present our algorithm for online trajectory generation. Our method involves the following steps:

A. Generating a collision free path

A collision free path from the current position of the quadrotor to the goal position is generated using the notion of 3D generalized shape given in [15]. This is given from Lines 2 to 19 of Algorithm 1. However the major difference is that instead of using the entire obstacle workspace to generate a collision free path, we use the local point cloud data and treat the unexplored workspace as obstacle-free. This reduces the on-board computation time.

B. Trajectory Optimization

The collision-free path computed using 3D-GSE [15] is piece-wise linear and is inefficient for quadrotor motion because the quadrotors have to stop at each waypoint in order to track the path. In this section, we present our trajectory optimization algorithm based on polynomial fitting, which transforms the piece-wise linear path into a smooth trajectory.

Consider the scenarios presented in Figs. 2b and 2c, where the agent is located at \mathbf{X} and the yellow region represents the conic hull $\widetilde{\mathcal{R}_{i,X}}$ in the direction of the obstacle. The region outside the conic hull is non-convex and is also a safe region. For simplicity, we compute a convex subset for g_i to generate a trajectory that lies inside the safe region. To compute a convex subset, we construct a plane with a normal such that it passes through \mathbf{X} . The convex 3D GSE shape is given as $\text{ConvexShape} = g_1 * g_2 * \dots * g_{m_{\text{loc}}}$ where, $g_i = h_i + c_{i-1} + c_{i-2} + \dots + c_1 - (i+1)$. The g_i 's are constructed in such a way that set of all points belonging to each $g_i = 0$ is convex. Since product of two or more functions are convex, $\text{ConvexShape} = g_1 * g_2 * g_{m_{\text{loc}}}$ is convex. Here,

c_i determines if the angle between $(\mathbf{P} - \mathbf{X})$ and $\mathbf{n}_{i,\mathbf{X}}$ for a point \mathbf{P} is greater than 90° . That is, c_i is given by,

$$c_i = \text{sat}(\cos^{-1}(\frac{\mathbf{n}_{i,\mathbf{X}} \cdot (\mathbf{P} - \mathbf{X})}{\|\mathbf{n}_{i,\mathbf{X}}\|_2 \|\mathbf{P} - \mathbf{X}\|_2}) - \pi/2) \quad (3)$$

$$\theta_{i,X} = \tan^{-1}(l_{i,X}/r_{i,X}) \quad (4)$$

$$h_i = \text{sat}(\theta_i - \cos^{-1}(\frac{\mathbf{n}_{i,\mathbf{X}} \cdot (\mathbf{P} - \mathbf{X})}{\|\mathbf{n}_{i,\mathbf{X}}\|_2 \|\mathbf{P} - \mathbf{X}\|_2})) + \text{sat}(r_{i,X} - \|\mathbf{P} - \mathbf{X}\|_2) \quad (5)$$

$$g_i = h_i + c_{i-1} + c_{i-2} + \dots c_1 - (i+1) \quad (6)$$

where $\text{sat}(x) = 1$ if $x \geq 0$ else 0. Now $c_i = 1$ if and only if a point lies in the blue region, as shown in Fig. 2c. The ConvexShape is computed by evaluating c_i and g_i for $i \in \{1, 2, \dots, m_{\text{loc}}\}$. We generate dynamically feasible trajectories by minimizing the snap similar to [16]. The entire trajectory is composed of m polynomials each of degree n , and the i^{th} trajectory is contained in C_{X_i} defined as follows,

$$C_{X_i} = \prod_{j=1}^{m_{\text{loc}}} g_j. \quad (7)$$

where \mathbf{X}_i , $i \in \{1, \dots, h\}$ are the waypoints of the collision-free path generated in the previous section and C_{X_i} is the 3D generalized shape generated about point \mathbf{X}_i and obtained using the convex subset of $g_j = 0$ where $j \in \{1, 2, \dots, m_{\text{loc}}\}$.

Consider a trajectory $\sigma(t)$ consisting of m piecewise polynomials $\sigma_i(t)$ for $i \in \{1, 2, \dots, m\}$ as a function of t and which have order n . The minimum snap optimization problem then becomes:

$$\begin{aligned} \underset{\sigma(t)}{\text{argmin}} \quad J &= \sum_{i=0}^{n-1} \int_{t_i}^{t_{i+1}} \left\| \frac{d^4}{dt^4} \sigma_i(t) \right\|^2 dt \\ \text{subject to} \quad & \frac{d^k}{dt^k} \sigma_i(t_i) = \frac{d^k}{dt^k} \sigma_{i+1}(t_i) \quad k = 0, \dots, 4 \\ & \left\| \frac{d}{dt} \sigma_{p,i}(t) \right\| \leq \mathbf{v}_{\text{max}}, \quad \left\| \frac{d^2}{dt^2} \sigma_{p,i}(t) \right\| \leq \mathbf{a}_{\text{max}} \quad i = 1, 2, \dots, m \\ & \sigma_i(t) \in C_{X_i} \end{aligned} \quad (8)$$

and the trajectories are parameterized using suitable basis functions in $\mathbb{R}^3 \times SO(2)$ which are piecewise polynomial functions as in [16] and is as follows:

$$\sigma(t) = \begin{cases} \sum_{i=1}^n \sigma_{1i} t^i & t_0 \leq t \leq t_1 \\ \sum_{i=1}^n \sigma_{2i} t^i & t_1 \leq t \leq t_2 \\ \dots \\ \sum_{i=1}^n \sigma_{mi} t^i & t_{m-1} \leq t \leq t_m \end{cases}$$

where $\sigma_{ij}(t) = [x_{ij}(t) \ y_{ij}(t) \ z_{ij}(t) \ \psi_{ij}(t)]$ is a vector of flat variables for a quadrotor and $\sigma_i(t) = [x_i \ y_i \ z_i \ \psi_i]$ and $\sigma(t)$ are piecewise polynomials as a function of time as defined above. $\sigma_i(t)$ can be rewritten as $\sigma_i(t) = [\sigma_{p,i}(t) \ \sigma_{o,i}(t)]$ where $\sigma_{p,i}(t) = [x_i \ y_i \ z_i]$ and $\sigma_{o,i}(t) = [\psi_i]$. Here the vector $[x_i \ y_i \ z_i]$ $i \in \{1, 2, \dots, m\}$ denotes the m way points generated by the online 3D-OGSE algorithm. The thrust constraints for the quadrotor can be directly related to the maximum acceleration constraints given in 8. The function TrajOpt in Line 17 of Algorithm

Algorithm 1 3D Online GSE Algorithm (3D-OGSE). Our novel online, 3D algorithm

```

1: while  $\|\mathbf{p} - \mathbf{X}_{\text{goal}}\| \leq \epsilon$  do
2:    $m_{\text{loc}} \leftarrow \text{SegmentLocalMap}(\mathbf{p})$  // obstacle data
3:    $\mathbb{V} \leftarrow \mathbb{V} \cup \{\mathbf{p}\}$ 
4:    $\mathbb{V} \leftarrow \mathbb{V} \cup \{\mathbf{X}_{\text{goal}}\}$ 
5:   while No directed graph is generated from  $\mathbf{p}$  to  $\mathbf{X}_{\text{goal}}$ 
     do
6:      $\mathbf{X}_{\text{rand}} \leftarrow \text{SamplePoint}$ 
7:      $\mathbf{X}_{\text{nearest}} \leftarrow \text{Nearest}(\mathbb{V}, \mathbf{X}_{\text{rand}})$ 
8:      $\mathbf{X}_{\text{new}} \leftarrow \text{Steer}(\mathbf{X}_{\text{rand}}, \mathbf{X}_{\text{nearest}})$ 
9:      $\mathbb{V} \leftarrow \mathbb{V} \cup \{\mathbf{X}_{\text{new}}\}$ 
10:     $\mathbb{E} \leftarrow \mathbb{E} \cup \{(\mathbf{X}_{\text{nearest}}, \mathbf{X}_{\text{new}})\}$ 
11:     $\mathbb{X}_{\text{near}} \leftarrow \text{NearIntersectedShapes}(G, \mathbf{X}_{\text{new}})$ 
12:    for  $\mathbf{X}_n \in \mathbb{X}_{\text{near}}$  do
13:       $\mathbb{E} \leftarrow \mathbb{E} \cup \{(\mathbf{X}_n, \mathbf{X}_{\text{new}})\}$ 
14:    end for
15:  end while
16:   $\text{Path} \leftarrow \text{dijkstra}(\mathbf{p}, \mathbf{X}_{\text{goal}}, G)$  // compute
    collision-free path
17:   $\text{Trajectory} \leftarrow \text{TrajOpt}(\text{Path}, \text{Shapes})$ 
18:   $\mathbb{V} \leftarrow \emptyset$  // clear vertex Set
19:   $\mathbb{E} \leftarrow \emptyset$  // clear edge Set
20:  while  $\text{Trigger}(\mathbf{p})=0$  do
21:     $\mathbf{p} \leftarrow \mathbf{p} + \frac{\frac{d\sigma(\mathbf{t}_0)}{dt}}{\|\frac{d\sigma(\mathbf{t}_0)}{dt}\|} \Delta$  //update agent position
22:  end while
23: end while

```

1 computes the trajectory by solving the optimization problem 8. It must be noted that the velocity and acceleration constraints for the quadrotor have been incorporated in the optimization problem to ensure dynamic feasibility.

C. Replanning triggering method

We build a global map from the current position to the goal position assuming that the unknown space is obstacle free. The update rate of getting the point cloud data is always greater than the update rate of the re-planning stage to ensure that the trajectories are collision-free. We present an online replanning triggering method. The trajectories are not continuously replanned as new point cloud data are received as this may be computationally expensive to do it onboard. We use the notion of generalized shape to replan trajectories only if they are necessary. Consider a quadrotor at its current position \mathbf{p} . Based on the point cloud data (say \mathbb{D}), let the generated trajectory be $\sigma(t)$. Let the next point to which the quadrotor moves be \mathbf{p}' , which is a distance Δ apart from \mathbf{p} along the trajectory. Now before the quadrotor moves to \mathbf{p}' , we check if the point \mathbf{p}' lies inside the 3D generalized shape computed about \mathbf{p} for the point cloud data \mathbb{D} . If the point is inside the generalized shape about \mathbf{p} , and \mathbf{p} is inside the generalized shape about \mathbf{p}' (using the same point cloud data \mathbb{D}) no replanning is done, else we replan the trajectory. This is summarized in Algorithm 2. Since the generalized shape represents the computed maximal free space available at any point, we observe that only a few replanning triggers are made before the agent reaches its goal position \mathbf{X}_{goal} .

Algorithm 2 Trigger(p)

```

1: Trajectory  $\sigma(t) \leftarrow \text{TrajOpt}(\text{Path}, \text{Shapes})$  //
   generate trajectory
2:  $p' \leftarrow p + \frac{d\sigma(t_0)}{\|d\sigma(t_0)\|} \Delta$ 
3: if GSE-Shape( $p', p, m_{\text{loc}}$ ) = 0 then
4:   if GSE-Shape( $p, p', m_{\text{loc}}$ ) = 0 then
5:     Trigger( $p$ ) = 0
6:   end if
7: else
8:   Trigger( $p$ ) = 1
9: end if
10: return Trigger( $p$ )

```

Since our proposed 3D-OGSE planner allows smoothness and continuity even in higher derivatives (Eqn. (8)), we are able to use the full state of the quadrotor, including velocity and acceleration constraints, guaranteeing smooth paths even in changing plans. The only constraint that can be enforced is the static one (all time derivatives are zero). However, in our method we first generate a feasible path from the current position to the goal position assuming the unknown space is obstacle-free and perform snap minimization. We can therefore guarantee that our generated trajectories are safe from Proposition 1. Since our approach allows better control over the end derivatives, we are able to continue planning from the exact current state of the quadrotor, leading to continuous and smooth paths.

Proposition 1: (Collision-Free Trajectories): The 3D-OGSE guarantees collision-free trajectories in cluttered 3D environments.

Proof: Consider a generalized shape \mathcal{G}_X about a point X . If an agent is at position $X \in \mathcal{G}_X$, by construction it implies that the agent would not collide with any obstacle. A collision-free path is computed using sampled points X_{rand} , where $X_{\text{rand}} \in \mathcal{G}_X$. Thus any path constructed from \mathbb{V} would not result in a collision. Further, a trajectory is generated from the collision-free path such that it lies within a conservative convex subset of \mathcal{G}_X . The workspace can be divided into two parts observed and unobserved as follows

$$\mathbb{X} = \mathbb{X}_{\text{observed}} + \mathbb{X}_{\text{unobserved}}$$

Let p be the current position of the quadrotor and $\sigma(t)$ be the trajectory generated when the quadrotor is at position p . Let the set \mathbb{S} be defined as follows

$$\mathbb{S} = \left\{ \gamma | x = p + \frac{\sigma(t_0)}{\|\sigma(t_0)\|} \gamma, x \in \mathcal{G}_p \text{ and } \gamma < \epsilon \right\}$$

Δ in Line 2 of Algorithm 2 is chosen in such a way that $\Delta = \max_{\gamma} \mathbb{S}$. Since $\mathcal{G}_p \in \mathbb{X}_{\text{free}} \cap \mathbb{X}_{\text{observed}}$ by construction, it implies that $x \in \mathbb{X}_{\text{free}} \cap \mathbb{X}_{\text{observed}}$. Therefore, the next point the quadrotor moves is always collision free. This is repeated until the quadrotor reached the goal point. Thus the trajectories are guaranteed to be collision-free.

D. Extension to Dynamic Scenes

Since our algorithm utilizes obstacle-free regions to re-plan a collision-free trajectory at each timestep, it can be

Method		Computation Time (ms)			Trajectory Cost (snap (m/s ⁴))
		Total Time	Path Computation	Trajectory Generation	
3D-OGSE	Mean	1.345	0.536	0.809	51.562
	Max	4.745	0.934	3.811	96.562
	Std	1.452	0.441	1.011	17.357
Liu et al. [13]	Mean	9.324	3.371	5.952	60.577
	Max	15.729	6.437	9.292	101.578
	Std	2.245	0.378	1.873	20.178
Gao and Shen [14]	Mean	13.547	5.509	8.038	62.189
	Max	25.265	10.638	14.627	105.272
	Std	4.352	1.283	3.069	12.467
Usenko et. al [33]	Mean	5.512	-	5.512	58.986
	Max	7.653	-	7.653	96.463
	Std	2.568	-	2.568	16.578

TABLE II: We tabulate the computation time and trajectory cost (snap) averaged over 100 generated trajectories for an agent operating in the random forest environment. We highlight the breakdown of the computation time between path generation and trajectory optimization for our algorithm 3D-OGSE and compare it with Liu et al. [13], Gao and Shen [14], and Usenko et. al [33]. Overall, we observe a 6 – 10 \times improvement in the performance over the prior methods, while our trajectory cost are comparable. Since Usenko et al. is purely a trajectory optimization based method, there is no path generation, thus the table entries for this case is empty.

extended to scenarios involving dynamic obstacles. Consider an quadrotor at a position p at timestep t_1 . The point cloud of the local environment generated at t_1 is segmented to m_{loc} obstacles which includes the dynamic obstacles. Our approach makes no assumption about m_{loc} and can handle new dynamic obstacles in its neighborhood in a real time manner. We use the current set of m_{loc} point clouds to compute a collision-free trajectory. During the next timestep t_2 , the dynamic obstacle may have moved to a new position, but this new position is captured in the point cloud generated at time t_2 . Hence the algorithm would still generate a new collision-free trajectory. Since our algorithm is fast and re-plans a trajectory at each timestep, it can react to moving obstacles in the environment and compute a new collision-free trajectory.

V. RESULTS

A. Implementation

Our method is implemented on an Intel Core i5-8500 CPU at 3.0 GHz with 32GB memory. We use ROS Melodic and Rviz for our simulation experiments. The trajectory optimization is performed using Mosek [32].

B. Comparison and Benefits

We evaluate our method in simulation with prior state-of-the-art online trajectory generation methods presented by Liu et al. [13], Gao and Shen [14] and Usenko et. al [33]. We present the benefits of our method in terms of its low computation time, trajectory cost, and better performance in narrow passages and in environments with high building densities.

1) *Computation Time and Trajectory Cost:* Table II compares the computation time and trajectory cost for 3D-OGSE with prior methods presented by Liu et al. [13], Gao et al. [14], and Usenko et al. [33]. The values tabulated are

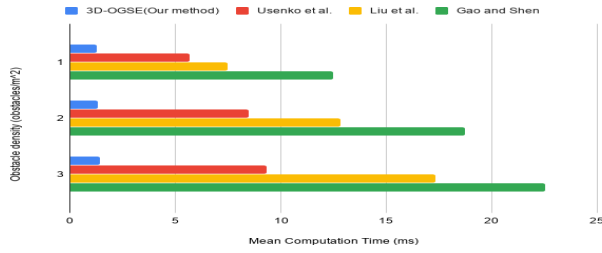


Fig. 3: Hundreds of trajectories are generated in 3D random forest environments with varying obstacle densities (obstacles per unit area) using our method and methods from Liu et al. [13], Gao and Shen [14], and Usenko et al. [33]. We observed that, as the obstacle density increases, the variation in the mean computation time for 3D-OGSE is less than the prior methods.

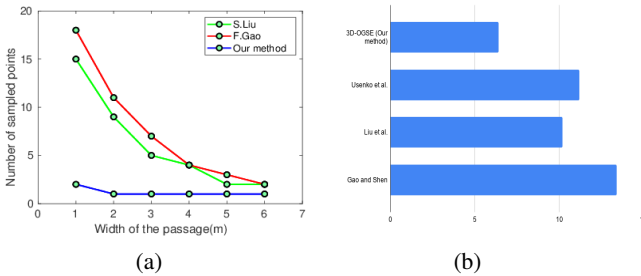


Fig. 4: (a): We compute a feasible path through a narrow passage of fixed length and progressively narrowing width. We observe that our method samples lower number of points for the narrow passage than Liu et al. [13] and Gao and Shen [14]. Fig. (b): We generate 100 trajectories in random forest environment and calculate the average number of replanning triggers using our method, Liu et al. [13], Gao and Shen [14] and Usenko et al. [33].

averaged over 100 generated trajectories, and the methods were compared in the random forest environment with the same start and goal positions. The maximum velocity and acceleration limits were taken as $3m/s$ and $2m/s^2$ respectively. It can be observed from Table II that the trajectory cost of 3D-OGSE is comparable to prior methods [13], [14], [33], while the computation time for our method is significantly lower.

2) *Obstacle Density*: Fig. 3 shows the variation in computation time with an increase in the environment’s obstacle density. For this scenario, the obstacle density increased from 1 to 3 obstacles/ m^2 . We observe that with an increase in obstacle density, the corresponding increase in computation time is significantly lower in our method than in Liu et al. [13], Gao et al. [14], and Usenko et al. [33]. The computation times reported are averaged over 100 generated trajectories.

3) *Narrow passages*: We evaluate the performance of the algorithms in multiple narrow passages of fixed length and different widths. Fig. 4a shows the variation in the number of sampled points (in the narrow passage) when computing a feasible path and the passage width. We observe in our method the number of sampled points remain almost constant with the decrease in passage width, while the number of

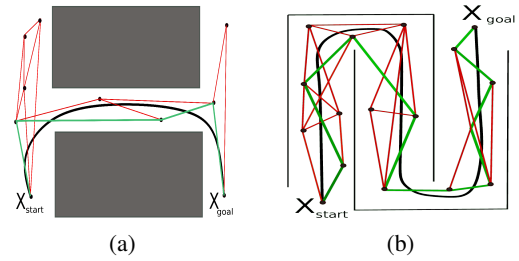


Fig. 5: A horseshoe environment and a thin corridor is considered. We observe that our proposed 3D-OGSE algorithm is able to generate a feasible trajectory from the start to goal location in these scenarios. The width of the passage in horseshoe environment and thin corridor is 1m. The green lines denote the shortest path from X_{init} to X_{goal} and black lines denote the smooth trajectory between these points

sampled points increases in [13], [14]. This is because the computed generalized shape in 3D-OGSE is relatively less conservative; hence, it requires fewer sample points to compute a path through the passage. Further in Fig. 5 we observe our algorithm perform well even in complex scenario’s such as the ‘horseshoe’ environment.

4) *Replanning Triggers*: We generated 100 trajectories from a start to goal position in the random forest environment for our proposed method, [13], [14] and [33]. The average number of replanning triggers required to reach the goal positions is then calculated for these 100 trajectories and is shown in Fig. 4b. We observe that our methods required lower number of replanning triggers than [13], [14], [33].

VI. CONCLUSION

In this letter, we propose a novel online trajectory generation algorithm, 3D-OGSE, for autonomous navigation of a quadrotor in an unknown environment. Our algorithm uses local depth information to continuously re-plan trajectories to direct the agent towards a goal position. Our algorithm is fast and requires 1.6 ms on average to re-plan trajectories, which is approximately 6-10x faster than [13], [14], and [33].

Our method has some limitations. We assume that the point cloud captures all the obstacles in the scene accurately and we are able to segment the point cloud data into individual obstacles. In addition, we require the accurate point cloud data and the quadrotor position in the environment. Furthermore, the quadrotor is represented as a point object. Our formulation of 3D-OGSE and computation of convex subsets can be conservative. We plan on extending our algorithm to stochastic settings, where trajectories are generated by taking sensor noise into account. Further, we plan on extending this method for scenarios with dynamic obstacles and evaluating the performance on a quadrotor system in real-world scenarios. Also we plan to incorporate medial axis with our proposed method to guarantee safety and maximum clearance with the obstacles. Good methods to compute approximate medial axis from sensor or point cloud data [34], [35], [36] and they can be combined with our formulation. This is useful in highly uncertain and cluttered environments and in practical applications where safety is the main concern.

REFERENCES

- [1] F. Liao, S. Lai, Y. Hu, J. Cui, J. L. Wang, R. Teo, and F. Lin, "3d motion planning for uavs in gps-denied unknown forest environment," in *2016 IEEE Intelligent Vehicles Symposium (IV)*. IEEE, 2016, pp. 246–251.
- [2] D. Scaramuzza, M. C. Achtelik, L. Doitsidis, F. Friedrich, E. Kosmatopoulos, A. Martinelli, M. W. Achtelik, M. Chli, S. Chatzichristofis, L. Kneip *et al.*, "Vision-controlled micro flying robots: from system design to autonomous navigation and mapping in gps-denied environments," *IEEE Robot. & Autom. Magazine*, vol. 21, no. 3, pp. 26–40, 2014.
- [3] F. Augugliaro, A. P. Schoellig, and R. D'Andrea, "Generation of collision-free trajectories for a quadcopter fleet: A sequential convex programming approach," in *2012 IEEE/RSJ Int. Conf. on Intelligent Robots and Systems*. IEEE, 2012, pp. 1917–1922.
- [4] Y. Chen, M. Cutler, and J. P. How, "Decoupled multiagent path planning via incremental sequential convex programming," in *2015 IEEE Int. Conf. on Robot. and Autom. (ICRA)*. IEEE, 2015, pp. 5954–5961.
- [5] A. Kushleyev, D. Mellinger, C. Powers, and V. Kumar, "Towards a swarm of agile micro quadrotors," *Autonomous Robots*, vol. 35, no. 4, pp. 287–300, 2013.
- [6] R. Deits and R. Tedrake, "Efficient mixed-integer planning for uavs in cluttered environments," in *2015 IEEE Int. Conf. on Robot. and Autom. (ICRA)*. IEEE, 2015, pp. 42–49.
- [7] B. MacAllister, J. Butzke, A. Kushleyev, H. Pandey, and M. Likhachev, "Path planning for non-circular micro aerial vehicles in constrained environments," in *2013 IEEE Int. Conf. on Robot. and Autom.* IEEE, 2013, pp. 3933–3940.
- [8] M. Likhachev and D. Ferguson, "Planning long dynamically feasible maneuvers for autonomous vehicles," *The Int. Journal of Robot. Research*, vol. 28, no. 8, pp. 933–945, 2009.
- [9] M. Pivtoraiko, D. Mellinger, and V. Kumar, "Incremental micro-uav motion replanning for exploring unknown environments," in *2013 IEEE Int. Conf. on Robot. and Autom.* IEEE, 2013, pp. 2452–2458.
- [10] S. Karaman and E. Frazzoli, "Sampling-based algorithms for optimal motion planning," *The Int. journal of Robot. research*, vol. 30, no. 7, pp. 846–894, 2011.
- [11] J. J. Kuffner Jr and S. M. LaValle, "Rrt-connect: An efficient approach to single-query path planning," in *ICRA*, vol. 2, 2000.
- [12] V. Zinage and S. Ghosh, "An efficient motion planning algorithm for uavs in obstacle-cluttered environment," in *2019 American Control Conf. (ACC)*. IEEE, 2019, pp. 2271–2276.
- [13] S. Liu, M. Watterson, K. Mohta, K. Sun, S. Bhattacharya, C. J. Taylor, and V. Kumar, "Planning dynamically feasible trajectories for quadrotors using safe flight corridors in 3-d complex environments," *IEEE Robot. and Autom. Letters*, vol. 2, no. 3, pp. 1688–1695, 2017.
- [14] F. Gao and S. Shen, "Online quadrotor trajectory generation and autonomous navigation on point clouds," in *2016 IEEE Int. Symposium on Safety, Security, and Rescue Robot. (SSRR)*. IEEE, 2016, pp. 139–146.
- [15] V. V. Zinage and S. Ghosh, "Generalized shape expansion-based motion planning for uavs in three dimensional obstacle-cluttered environment," in *AIAA Scitech 2020 Forum*, 2020, p. 0860.
- [16] D. Mellinger and V. Kumar, "Minimum snap trajectory generation and control for quadrotors," in *2011 IEEE Int. Conf. on Robot. and Autom.* IEEE, 2011, pp. 2520–2525.
- [17] M. Zucker, N. Ratliff, A. D. Dragan, M. Pivtoraiko, M. Klingensmith, C. M. Dellin, J. A. Bagnell, and S. S. Srinivasa, "Chomp: Covariant hamiltonian optimization for motion planning," *The Int. Journal of Robot. Research*, vol. 32, no. 9–10, pp. 1164–1193, 2013.
- [18] Y. Lin, F. Gao, T. Qin, W. Gao, T. Liu, W. Wu, Z. Yang, and S. Shen, "Autonomous aerial navigation using monocular visual-inertial fusion," *Journal of Field Robot.*, vol. 35, no. 1, pp. 23–51, 2018.
- [19] S. Liu, N. Atanasov, K. Mohta, and V. Kumar, "Search-based motion planning for quadrotors using linear quadratic minimum time control," in *2017 IEEE/RSJ Int. Conf. on Intelligent Robots and Systems (IROS)*. IEEE, 2017, pp. 2872–2879.
- [20] L. E. K. J.-C. Latombe, "Probabilistic roadmaps for robot path planning," *Practical motion planning in Robot.: current approaches and future challenges*, pp. 33–53, 1998.
- [21] S. M. LaValle and J. J. Kuffner Jr, "Randomized kinodynamic planning," *The Int. journal of Robot. research*, vol. 20, no. 5, pp. 378–400, 2001.
- [22] J. Yu, Z. Cai, and Y. Wang, "Minimum jerk trajectory generation of a quadrotor based on the differential flatness," in *Proceedings of 2014 IEEE Chinese Guidance, Navigation and Control Conf.*, Aug 2014, pp. 832–837.
- [23] D. Morgan, S.-J. Chung, and F. Y. Hadaegh, "Decentralized model predictive control of swarms of spacecraft using sequential convex programming," *Advances in the Astronautical Sciences*, no. 148, pp. 1–20, 2013.
- [24] H. Zhu and J. Alonso-Mora, "Chance-constrained collision avoidance for mavs in dynamic environments," *IEEE Robot. and Autom. Letters*, vol. 4, no. 2, pp. 776–783, April 2019.
- [25] M. Kamel, J. Alonso-Mora, R. Siegwart, and J. Nieto, "Robust collision avoidance for multiple micro aerial vehicles using nonlinear model predictive control," in *2017 IEEE/RSJ Int. Conf. on Intelligent Robots and Systems (IROS)*, Sep. 2017, pp. 236–243.
- [26] C. R. Qi, H. Su, K. Mo, and L. J. Guibas, "Pointnet: Deep learning on point sets for 3d classification and segmentation," in *Proceedings of the IEEE Conf. on Computer Vision and Pattern Recognition*, 2017, pp. 652–660.
- [27] Q. Huang, W. Wang, and U. Neumann, "Recurrent slice networks for 3d segmentation of point clouds," in *Proceedings of the IEEE Conf. on Computer Vision and Pattern Recognition*, 2018, pp. 2626–2635.
- [28] H.-Y. Meng, L. Gao, Y.-K. Lai, and D. Manocha, "Vv-net: Voxel vae net with group convolutions for point cloud segmentation," in *Proceedings of the IEEE International Conference on Computer Vision*, 2019, pp. 8500–8508.
- [29] M. Fliess, J. Lévine, P. Martin, and P. Rouchon, "Flatness and defect of non-linear systems: introductory theory and examples," *Int. journal of control*, vol. 61, no. 6, pp. 1327–1361, 1995.
- [30] V. Hagenmeyer and E. Delaleau, "Exact feedforward linearization based on differential flatness," *Int. Journal of Control*, vol. 76, no. 6, pp. 537–556, 2003.
- [31] D. Mellinger and V. Kumar, "Minimum snap trajectory generation and control for quadrotors," in *2011 IEEE Int. Conf. on Robot. and Autom.* IEEE, 2011, pp. 2520–2525.
- [32] "Mosek aps." [Online]. Available: <https://www.mosek.com/>
- [33] V. Usenko, L. von Stumberg, A. Pangercic, and D. Cremers, "Real-time trajectory replanning for mavs using uniform b-splines and a 3d circular buffer," in *2017 IEEE/RSJ Int. Conf. on Intelligent Robots and Systems (IROS)*. IEEE, 2017, pp. 215–222.
- [34] J. Ma, S. Bae, and S. Choi, "3d medial axis point approximation using nearest neighbors and the normal field," *The Visual Computer*, vol. 28, pp. 7–19, 01 2012.
- [35] A. Sud, M. Foskey, and D. Manocha, "Homotopy-preserving medial axis simplification," *International Journal of Computational Geometry & Applications*, vol. 17, no. 05, pp. 423–451, 2007.
- [36] A. Tagliasacchi, T. Delame, M. Spagnuolo, N. Amenta, and A. Telea, "3d skeletons: A state-of-the-art report," in *Computer Graphics Forum*, vol. 35, no. 2. Wiley Online Library, 2016, pp. 573–597.